ChemPubSoc Europe

DOI: 10.1002/cphc.201201044

Unbiased Photoelectrochemical Water Splitting in Z-Scheme Device Using W/Mo-Doped $BiVO_4$ and $Zn_xCd_{1-x}Se$

Hyun S. Park, Heung Chan Lee, Kevin C. Leonard, Guanjie Liu, and Allen J. Bard*[a]

Photoelectrochemical water splitting to generate H_2 and O_2 using only photon energy (with no added electrical energy) has been demonstrated with dual n-type-semiconductor (or Z-scheme) systems. Here we investigated two different Z-scheme systems; one is comprised of two cells with the same metal-oxide semiconductor (W- and Mo-doped bismuth vanadate), that is, Pt-W/Mo-$BiVO_4$, and the other is comprised of the metal oxide and a chalcogenide semiconductor, that is, Pt-W/Mo-$BiVO_4$ and $Zn_{0.2}Cd_{0.8}Se$. The redox couples utilized in these Z-scheme configurations were I^-/IO_3^- or S^{2-}/S_n^{2-}, respectively. An electrochemical analysis of the system in terms of cell components is shown to illustrate the behavior of the complete photoelectrochemical Z-scheme water-splitting system. H_2 gas from the unbiased photolysis of water was detected using gas chromatography–mass spectroscopy and using a membrane-electrode assembly. The electrode configuration to achieve the maximum conversion efficiency from solar energy to chemical energy with the given materials and the Z-scheme is discussed. Here, the possibilities and challenges of Z-scheme unbiased photoelectrochemical water-splitting devices and the materials to achieve practical solar-fuel generation are discussed.

1. Introduction

We show solar-fuel, that is H_2, generation from true splitting of water (H_2 and O_2 formation) without external bias or sacrificial donors in a photoelectrochemical (PEC) device using two identical metal-oxide photoelectrodes or a combination of one chalcogenide and one metal-oxide photoelectrode. These PEC devices demonstrate a conceptual design of unbiased water splitting using only photon energy at the photoelectrodes. PEC reactions, that is, the hydrogen evolution reaction (HER) and oxygen evolution reaction (OER), occur on the interface between a semiconductor electrode, usually with an electrocatalyst, and a solution with a suitable counter electrode. The semiconductor electrode absorbs photons with a higher energy than its band gap and the absorbed energy excites a bonding electron of the semiconductor to the conduction band with a hole left in the valence band. The excited electron and hole are separated by the electric field created near the interface between the semiconductor and solution. Through the reactions on the semiconductor, the absorbed radiant energy is converted and stored as chemical energy, for example, H_2 and O_2 from the photolysis of water.[1,2]

Efficiently and inexpensively converting radiant energy to chemical energy, and especially the water-splitting reaction, has been a great challenge for many decades as the ultimate solution of a sustainable energy source.[3] To attain the practical photolysis of water in an economical way, a) the semiconductor must be stable and not experience decomposition from the strong reductive and oxidative power of the excited electron and hole, b) the band gap of the semiconductor must be small enough to utilize most of the solar energy spectrum but large enough to drive the desired chemical reaction, and c) the semiconductor must have suitable positions of band edges for the chemical reactions of interest. In addition to those chemical and electrochemical criteria, the material should be abundant and inexpensive so the total system of water photolysis can compete with other energy-conversion systems, for example, H_2 production by electrolysis using photovoltaic solar cells, steam reforming from fossil fuels, or pyrolysis of biomass.[4] Typical rough benchmarks generally quoted are 10% solar efficiency, ten-year lifetime and installed power of $1 per watt.[3]

After Fujishima and Honda suggested the possible photolysis of water using a TiO_2 photoanode,[5] tremendous efforts have been made to realize water splitting using solar energy. A major part of the research focused on finding a single useful material for this reaction, mostly based on large band gap metal oxide semiconductors like TiO_2, $SrTiO_3$, and others.[6–10] For example, Youngblood et al. reported a steady photocurrent of 1 to 2 μA at a biased TiO_2 electrode with ruthenium dyes for water photolysis under visible irradiation.[6] A TiO_2 electrode coated with molecular catalysts and dye sensitizers was also demonstrated to produce about 5 $\mu A\,cm^{-2}$ photocurrent density for water oxidation without an external bias[8] and InP electrodes decorated with iron-complex catalysts generated about 250 $nA\,cm^{-2}$ for hydrogen evolution with an external bias under visible irradiation.[11] However, the needed driving force for water splitting is probably in the vicinity of 1.9 to 2 V, which is clearly significantly larger than the often-quoted ther-

[a] Dr. H. S. Park, Dr. H. C. Lee, Dr. K. C. Leonard, Dr. G. Liu, Prof. Dr. A. J. Bard
Center for Electrochemistry
Department of Chemistry and Biochemistry
The University of Texas at Austin
Austin, TX 78712 (USA)
E-mail: ajbard@mail.utexas.edu

Supporting information for this article is available on the WWW under http://dx.doi.org/10.1002/cphc.201201044.

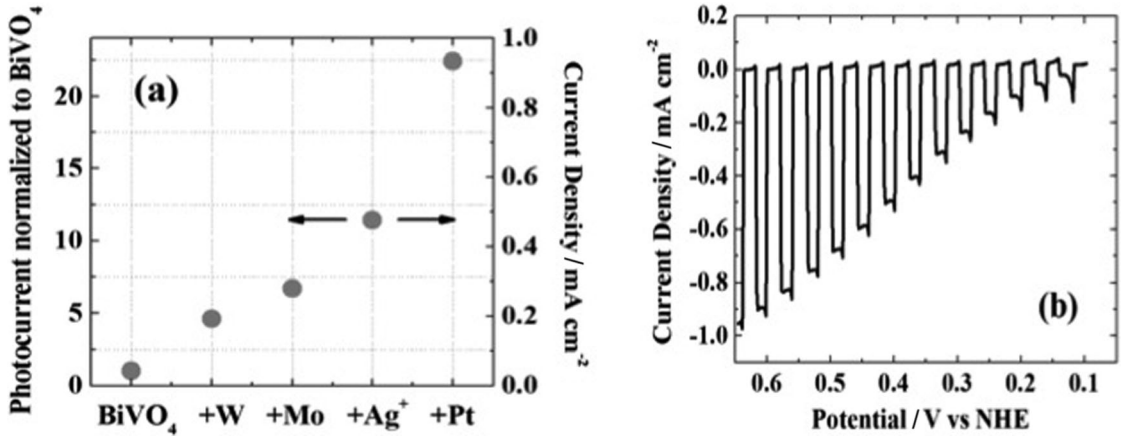

Figure 1. a) Summary of the photoactivity development of $BiVO_4$ and b) LSV of Pt-W/Mo-$BiVO_4$ for water oxidation under chopped UV/Vis irradiation. The photocurrent was measured for water oxidation in neutral aqueous solution (pH 7, 0.2 M phosphate buffered, 0.1 M Na_2SO_4) under 120 mW cm^{-2} UV/Vis irradiation. The photocurrent shown in (a) was chosen from the LSVs at 0.6 V (vs NHE) for different electrodes. The scan rate was 20 mV s^{-1}. Thin film electrodes of $BiVO_4$ or doped $BiVO_4$ were prepared by drop-casting precursor solution, and the thickness of the resulting films was about 0.5 μm. W-doped $BiVO_4$ has a 5 atomic% W to (Bi + V) ratio and W/Mo-doped $BiVO_4$ has a 2 atomic% W and 6% Mo to (Bi + V) ratio. For $AgNO_3$ treatment, W/Mo-$BiVO_4$ film was soaked in 10 mM $AgNO_3$ aqueous solution for 1 hr in the dark. Pt electrocatalyst was photodeposited under UV/Vis irradiation for 30 min in 10 mM H_2PtCl_4 in the presence of 0.2 M MeOH.

modynamic value of 1.23 V; this requires a semiconductor band gap that can only absorb a relatively small portion of the solar spectrum and hence a low efficiency of solar-energy conversion. To obtain a reasonable efficiency using smaller band-gap materials, two or more photons must be absorbed to drive a single electron in the reaction. Other systems have been suggested, for example, buried p–n junction electrodes,[12–14] tandem structures with dye-sensitized solar cells and a metal oxide,[15] and multiple bipolar photoelectrodes in a series connection,[16–18] where two or more semiconductors are combined to cover a wide solar-wavelength window and create a sufficient potential to drive the water-splitting reaction.

Among proposed systems, a dual n-type-semiconductor device (or Z-scheme) was suggested in 1979 to overcome the single photoelectrode problem.[19] Since that time, several efforts have been made to find a suitable combination of photoelectrodes and redox couples to demonstrate PEC water splitting by a Z-scheme.[20] Combinatorial methods have been explored as a quick screening method to find suitable photoanodes for water oxidation which utilize metal oxides,[21] for example, Fe_2O_3,[22–25] WO_3,[26,27] $BiVO_4$,[28,29] and chalcogenides, e.g., CdSe, $CuInSe_2$, and Cu_2ZnSnS-Se.[30–32]

The photocatalytic activity of $BiVO_4$ was first reported by Kudo and co-workers in 1999,[33] and has been studied as a promising material for photo-oxidation of water because it has good chemical stability and the ability to harvest visible radiation.[34,35] $BiVO_4$ is a yellow pigment and was first reported as a naturally existing mineral in 1974.[36] Moreover, as described above, the photoactivity of $BiVO_4$ has been improved significantly employing the combinatorial method utilized by our group. Scanning electrochemical microscopy (SECM) has been used to screen metal dopants for $BiVO_4$, for example, W and Mo,[26,27] which significantly improve the photoactivity of $BiVO_4$. In addition, our group has determined that Pt and cobalt oxides are good water oxidation electrocatalysts for W-doped $BiVO_4$.[36] As a result, W and Mo-doped $BiVO_4$ treated with $AgNO_3$[35] to passivate surface recombination and photodeposited with Pt, denoted Pt-W/Mo-$BiVO_4$, shows more than a 20-times-enhanced photocurrent for the OER compared to that of untreated $BiVO_4$ (Figure 1a).

In this paper, unbiased water splitting using a Z-scheme system is demonstrated using either two Pt-W/Mo-$BiVO_4$ photoelectrodes or a combination of $Zn_{0.2}Cd_{0.8}Se$ and Pt-W/Mo-$BiVO_4$ to capture the light. The redox couples used in the Z-scheme configuration were I^-/IO_3^- for Pt-W/Mo-$BiVO_4$ electrodes or S_n^{2-}/S^{2-} for $Zn_{0.2}Cd_{0.8}Se$ electrodes. Electrochemical analysis to determine the maximum photon conversion efficiency to chemical energy was also performed with the given photoelectrodes in a PEC device. Finally, the possibilities and challenges of using a Z-scheme system for unbiased photoelectrochemical water splitting and the materials necessary to achieve practical solar-fuel generation are discussed.

Experimental Section

Chemicals

$Bi(NO_3)_3{\cdot}5H_2O$ (99.999%), $(NH_4)_{10}H_2(W_2O_7)_6{\cdot}xH_2O$ (99.99%), and $Na_2S{\cdot}9H_2O$ (98%) were obtained from Strem Chemicals (Newburyport, MA). $H_2PtCl_6{\cdot}6H_2O$ (99.9%), VCl_3 (99%), $Cd(NO_3)_2{\cdot}4H_2O$ (99.999%), and Ti foil (2.0 mm thick, 99.2%) were purchased from Alfa-Aesar (Ward Hill, MA). $(CH_3)_2NC(Se)NH_2$ (97%), Se (100 mesh, 99.5%), $(NH_4)_6Mo_7O_{24}{\cdot}4H_2O$ (99.98%), Na_2SO_4 (99.0%), $Ag(NO_3)$ (99%), $CoCl_2$ (98%), and Nafion perfluorinated resin solution (5 wt% in lower aliphatic alcohols and water) were purchased from Sigma–Aldrich (St. Louis, MO). $ZnCl_2$ (98.55%), S (99.5%), and $NaIO_3$ (99.9%) were obtained from Mallinckrodt Baker (Phillipsburg, NJ). Na_2HPO_4 (99.9%), NaH_2PO_4 (99.5%), methanol (99.9%), isopropanol (99.5%), and ethylene glycol (99%) were purchased from Fisher Scientific (Pittsburg, PA). NaI (99%, EM Science, Gibbstown, NJ) were used as received. Fluorine-doped tin oxide (FTO, TEC 15, Pil-

kington, Toledo, OH) was used as the substrate for the film electrodes. Deionized Milli-Q water (D.I. water, 18 MΩ-cm) was used as the solvent in electrochemical experiments. Pt electrocatalyst supported on carbon (40 wt%, Pt/C, Johnson Matthey, London, UK) and a sulfonated tetrafluoroethylene membrane (51 μm thick, Nafion112, DuPont, Wilmington, DE) were used as received to prepare the membrane electrode assemblies.

Electrodes

Pt-W/Mo-doped $BiVO_4$ electrodes were prepared as previously described.[27,36] Briefly, a 20 μM $(NH_4)_{10}H_2(W_2O_7)_6{\cdot}xH_2O$, 60 μM $(NH_4)_6Mo_7O_{24}{\cdot}4H_2O$, 4.2 mM $Bi(NO_3)_3{\cdot}5H_2O$, and 5 mM VCl_3 in ethylene glycol solution was prepared. Then, 200 μL of the precursor solution was applied onto an FTO substrate (2.2 cm^2) and it was annealed at 500 °C for 3 h. The temperature was slowly ramped from room temperature to 500 °C over 9 h. Then, the W/Mo-$BiVO_4$ film was treated in a 10 mM $Ag(NO_3)_3$ aqueous solution in the dark for 1 h.[37] The Pt electrocatalyst was photodeposited as previously reported.[38] The metal-oxide film was placed in a 0.2 M MeOH and 10 mM H_2PtCl_6 aqueous solution and, while submerged, it was irradiated with a xenon lamp (XBO 150 W, Osram, Munich, Germany) for 30 min with full output. The irradiation power was about 150 mW cm^{-2}.

$Zn_{0.2}Cd_{0.8}Se$ electrodes were prepared using a drop-casting technique.[28] A 70 mM $ZnCl_2$, 0.5 M $Cd(NO_3)_2$, and 0.5 M $N(CH_3)_2NH_2CSe$ (dimethylselenourea) ethylene glycol solution was prepared and 0.1 M hydrazine was added to this solution to prevent the oxidation of dimethylselenourea by dissolved O_2 in the ethylene glycol. In addition to preventing oxidation, hydrazine provides a possible chemical combustion during low temperature selenization of $Zn_{0.2}Cd_{0.8}Se$.[39] To form a uniform film of chalcogenide, multiple drop-casted coats (usually three) were applied. For each coat, 50 μL of the precursor solution was applied to the surface of the FTO (1 cm^2) substrate. Then, the film was placed into a pre-heated oven to evaporate the solvent at 140 °C for about 30 min in ambient air. Finally, the film was annealed at 350 °C for 30 min under Ar flow with a flow rate of about 10 mL min^{-1} in a tube furnace. The ramping rate of the furnace temperature was 20 °C min^{-1} beginning from room temperature. To prevent excess loss of Se from the film, around 0.2 g of selenium powder was placed beside the film and it was usually completely evaporated during the selenization. By selenization, the color of the $Zn_{0.2}Cd_{0.8}Se$ film was changed from dark red to dark grey.

CoS electrodes were prepared on polished Ti foil (1.5 cm^2). The Ti foil was alternately dipped into the 0.5 M $CoCl_2$ and 0.5 M Na_2S aqueous solutions to form a powdery CoS film. After multiple coats of CoS, the film was annealed at 100 °C for 12 h with a ramp rate of 1 °C min^{-1} beginning from room temperature. The heat treatment was conducted under Ar flow with a flow rate of 10 mL min^{-1}.

The membrane-electrode assembly used for H_2 detection consisted of Pt/C electrocatalyst and a proton-conductive membrane as a solid electrolyte. The membrane was sulfonated by soaking the membrane in a 0.1 M aqueous sulfuric acid solution at boiling temperature for 1 h. After washing the sulfonated membrane with deionized water, the membrane was firmly secured between two glass plates where 1 cm × 2 cm windows were allowed to dry the membrane. Then, Pt/C electrocatalyst suspended in isopropanol with Nafion resin (30 wt% of Nafion resin to Pt/C) was sprayed onto the dried Nafion membrane using a spray gun (GP-1, Fuso Seiki Co., Tokyo, Japan). N_2 gas was used as the carrier medium for the deposition and both sides of the membrane were sprayed at room temperature.

Instruments

A CH Instruments model 630D electrochemical analyzer (Austin, TX) was used as a potentiostat for the electrochemical experiments. A Pt gauze counter electrode and a Ag/AgCl reference electrode in saturated KCl solution were used to complete the three-electrode configuration. It should be noted that all reported potentials in the three-electrode configuration are quoted with respect to the normal hydrogen electrode (NHE). For the PEC measurements, illumination was done with a xenon lamp (XBO 150 W, Osram, Munich, Germany) with full output for the UV/Vis irradiation, or with a 420 nm cut-off filter (WBF-3, Oriel, Darmstadt, Germany) for the visible irradiation. A silicon photodetector (Model 818-UV, Newport, Irvine, CA) with an attenuator (OD3, Newport) and an optical power meter (Model 1815-C and Model 1830-C, Newport) were used to obtain light intensities. A gas chromatography–mass spectroscopy analyzer (GC-2014, Shimadzu Scientific Instruments, Columbia, MD) was used to analyze the gases produced from the PEC device. The electrochemical cells for water splitting were home-built with borosilicate glass (Figure 3 and Supporting Information, Figure S1).

2. Results and Discussion

2.1. Pt-W/Mo-$BiVO_4$ Photoanode

A linear-sweep voltammogram (LSV) of Pt-W/Mo-$BiVO_4$ is shown in Figure 1 b for the OER. LSV measured under chopped UV/Vis irradiation with an intensity of 120 mW cm^{-2} shows rapid photoresponses. A current density of about 1 mA cm^{-2} was obtained at 0.6 V beyond the photo-onset potential of the OER for Pt-W/Mo-$BiVO_4$ in neutral aqueous solution (0.1 M Na_2SO_4, pH 7, 0.2 M sodium phosphate buffered) at 120 mW cm^{-2}. Figure 2 a-ii also shows the photocurrent for the OER under stronger irradiation (440 mW cm^{-2}) than that in Figure 1 b for the identical Pt-W/Mo-$BiVO_4$ electrode. The photocurrent increased about four times as the light intensity increased from 120 to 440 mW cm^{-2} in Figure 2 a. Some of the results shown utilize this stronger illumination intensity to shorten the experimental time necessary to detect the generated gases on the electrodes. The irradiation power as measured by the optical power meter is noted in each experiment. The LSV in Figure 2 a indicates that photocurrent for the OER on Pt-W/Mo-$BiVO_4$ begins around 50 mV vs NHE (line ii) demonstrating that the onset potential for the OER is largely shifted to the negative (by about 0.7 V) compared with the thermodynamic potential of O_2 evolution from water (0.81 V at pH 6).

In Figure 2 a, the proton reduction current begins at −0.4 V on a Pt electrode (black line, iii) which is very close to the thermodynamic potential for proton reduction, Equation (1), in a neutral aqueous solution and consistent with the rapid kinetics of the HER on Pt:

$$2H^+ + 2e \rightarrow H_2 \quad (E^0 = -0.41\ \text{V at pH 7}) \qquad (1)$$

From the respective LSVs for the half reactions of water splitting, that is, O_2 evolution (ii) and H_2 evolution (iii) as shown in Figure 2 a, the current density for water electrolysis under

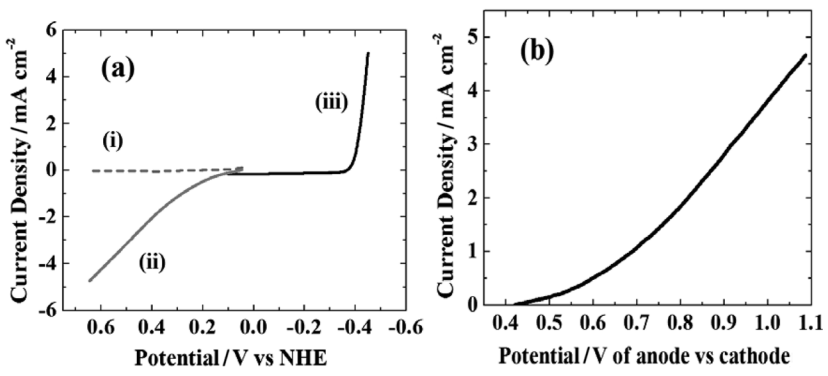

Figure 2. a) LSVs of Pt-W/Mo-$BiVO_4$ for water oxidation under dark (i) and under UV/Vis irradiation with radiation of intensity of about 440 mW cm^{-2} (ii). Iii) Current for proton reduction measured with a Pt mesh electrode. The current was measured in 0.1 M Na_2SO_4 aqueous solution (pH 7, 0.2 M sodium phosphate buffered). The scan rate was 20 mV s^{-1}. b) Current density and potential relationship calculated from the data shown in (a) showing the water-splitting current density for both proton reduction and water oxidation in a two-electrode system as a function of the applied potential difference between Pt-W/Mo-$BiVO_4$ and Pt electrodes in neutral aqueous solution.

UV/Vis irradiation using Pt-W/Mo-$BiVO_4$ and Pt is calculated as a function of the potential difference between the photoanode and the cathode in Figure 2b. For example, to obtain a current density of 4 mA cm^{-2} in a two electrode configuration, H_2 generation occurs at −0.44 V (vs NHE), and the same current must flow through the anode for oxygen evolution at 0.58 V (vs NHE) as shown in Figure 2a. This indicates that an electrochemical potential difference of 1 V (or 0.58 V − (−0.44 V)) needs to be applied between the anode and cathode to balance the electrochemical reactions in this two-electrode system and generate a 4 mA current (Figure 2b). Thus, the minimum potential difference that must be applied between the Pt-W/Mo-$BiVO_4$ and the Pt electrodes to initiate water splitting under irradiation is about 0.4 V.

The additional potential needed in a PEC system not connected to an external power source can be supplied by a buried junction (e.g. one or more *p*-n junction semiconductor devices) or by another PEC cell, operating with a mediator (O,R). As shown in Figure 3, a pair of n-type semiconductors (semiconductor I (SCI) and semiconductor II (SCII)) can thus accomplish the photolysis of water in a Z-scheme.[17] Briefly, SCII and the metal electrode I (MI) are used for water splitting with the OER on SCII and the HER on MI in an aqueous solution. The other electrodes (SCI and MII) are used to absorb and convert additional photon energy to electric energy by carrying out reduction and oxidation reactions in a separate cell containing an appropriate redox couple. For the system described here, Pt-W/Mo-$BiVO_4$ and Pt electrodes are used as SCII and MI as described above.

The redox couple O/R used was I^-/IO_3^-; this has been studied for photocatalytic water splitting by Abe et al. utilizing $SrTiO_2$, TiO_2, WO_3, and $BiVO_4$ powder.[40] They reported this redox couple was stable for prolonged experimental times. Thus the cell involved photooxidation of I^- on SCI (Pt-W/Mo-$BiVO_4$) and reduction of IO_3^- on MII (Pt).

LSVs for I^-/IO_3^- redox reactions in aqueous solution (25 mM/25 mM, pH 8.5) are shown in Figure 4a. Reduction of IO_3^- occurs on Pt electrodes and the reduction current starts at 0.6 V with possible reactions listed below. The thermodynamic potentials below, Equations (2)–(4), are calculated from the Nernst equation for pH 8.5:[41]

$$2IO_3^- + 12H^+ + 10\ e^- \rightarrow I_2 + 6H_2O\ (E^0 = 0.59\ V \text{ at pH } 8.5) \quad (2)$$

$$IO_3^- + 6H^+ + 6e^- \rightarrow I^- + 3H_2O\ (E^0 = 0.58\ V \text{ at pH } 8.5) \quad (3)$$

$$I_2 + 2e^- \rightarrow 2I^-\ (E^0 = 0.54\ V \text{ at pH } 8.5) \quad (4)$$

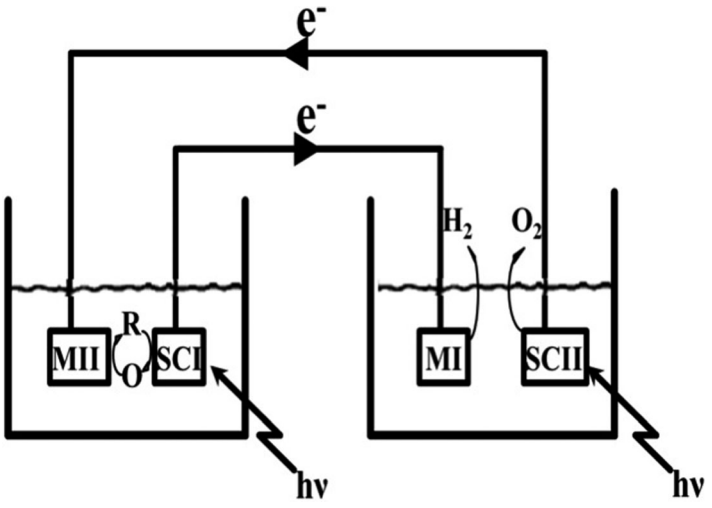

Figure 3. Schematic diagram of a dual n-type-semiconductor (SCI: semiconductor I, SCII: semiconductor II) system. Two metal electrodes (MI: metal I, MII: metal II) are used with the redox couple (R/O).

Photocurrent from the Pt-W/Mo-$BiVO_4$ electrode for the oxidation of I^- or I_2 (I_2 can be an intermediate, for example, from reaction of I^- with IO_3^-) to IO_3^- starts at about 0 V (shown in Figure 4a-iii). The onset potential of photooxidation agrees with the observed flat-band potential for the OER at a similar pH in Figure 2a. The reduction current from the I^-/IO_3^- redox couple starts to flow at about 0.6 V on the Pt electrode, which is more positive than the onset potential of photooxidation on Pt-W/Mo-$BiVO_4$. Thus, the reduction and oxidation reactions of the I^-/IO_3^- redox couple can happen spontaneously under irradiation because the thermodynamic redox potential of I^-/IO_3^- is located within the band gap of Pt-W/Mo-$BiVO_4$. As the photogenerated electron/hole pairs are

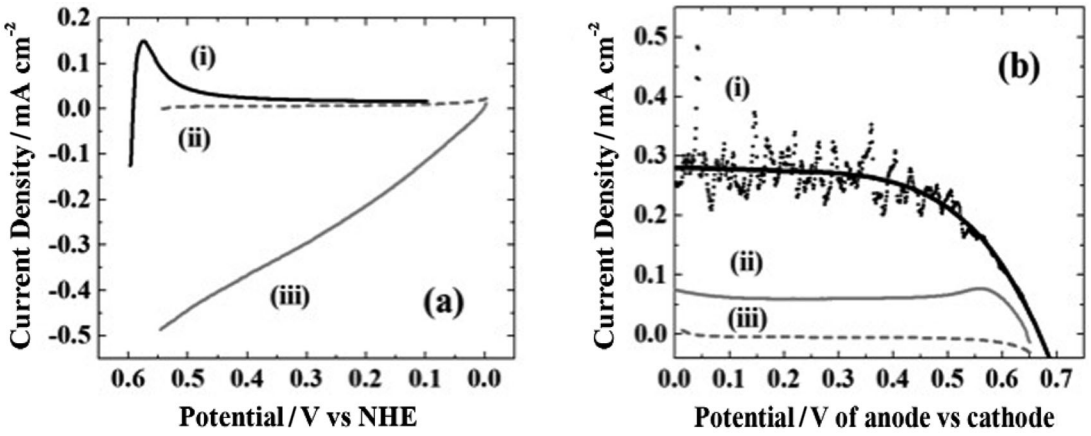

Figure 4. a) LSVs of IO_3^- reduction on Pt (scan from 0.6 to 0.1 V) (i) and I^- oxidation on Pt-W/Mo-$BiVO_4$ under dark (ii) and UV-visible irradiation (iii). b) LSVs in a two electrode configuration using Pt and Pt-W/Mo-$BiVO_4$ for I^-/IO_3^- redox reactions. Scan rate was 20 mV s^{-1}. Photocurrent flows under UV-visible irradiation with magnetic stirring (i) without stirring (ii) and in the dark (iii). The measurements were conducted in 25 mM NaI and 25 mM $NaIO_3$ aqueous solution (pH 8.5). Light intensity was about 400 mW cm^{-2}.

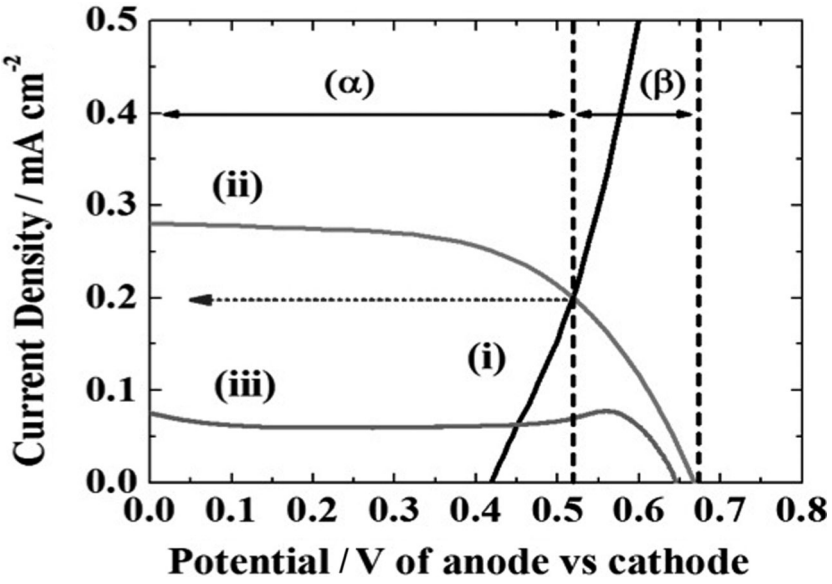

Figure 5. Overlapped LSVs of water splitting at Pt-W/Mo-$BiVO_4$ (i) and I^-/IO_3^- redox reactions with magnetic stirring (ii) and without stirring (iii) under UV/Vis irradiation with an intensity of about 400 mW cm^{-2}. Data was taken from Figure 2b and Figure 4b. In the plot, the current density for water splitting in the Z-scheme is estimated as 0.2 mA cm^{-2} (arrow) under strong UV/Vis irradiation with stirring for I^-/IO_3^- solution. This indicates about 0.5 V (α) of the generated potential from I^-/IO_3^- (from 0.7 V OCP) supplements the needed potential for proton reduction n on Pt with the remaining 0.2 V (β) driving the I^-/IO_3^- reaction in the galvanic cell.

produced on Pt-W/Mo-$BiVO_4$, the electron in the conduction band is delivered to the Pt electrode at a potential sufficiently negative to reduce IO_3^- while the hole in the valence band of the metal oxide electrode has a potential positive enough to oxidize I^- to IO_3^-.

Figure 4b shows the current–potential behavior under UV/Vis irradiation in a two-electrode configuration using Pt-W/Mo-$BiVO_4$ and Pt electrodes with the I^-/IO_3^- redox couple in aqueous solution. The two-electrode cell generates about 0.7 V open circuit potential (OCP) when no current flows and it produces about 0.3 mA cm^{-2} of photocurrent with magnetic stirring or 0.1 mA cm^{-2} without stirring of the solution when the two electrodes were short-circuited. Stirring causes an increase in the current because mass transport by diffusion is limited by the low solubility of IO_3^- or I_2. The OCP represents the maximum electrical energy obtained from the absorbed photon. A larger potential could be obtained if a redox couple with a more positive E^o would be available.

In Figure 5, the current–potential behavior for water splitting (i) and the redox reactions (ii and iii) in the two-electrode configuration are shown. When the four electrodes are connected as shown in Figure 3, the same current flows through all of the electrodes. Therefore, the crossing point of lines (i) and (ii) indicates the operating current of the Z-scheme device. In other words, an equivalent number of electrons must be used for H^+ and IO_3^- reduction on MI and MII, respectively, and the same number of holes must be used for I^- oxidation on SCI and the OER on SCII at the same time. Under this condition, the estimated current density for the water-splitting system as described here is 0.2 mA cm^{-2} (red arrow). The I^-/IO_3^- cells (open circuit voltage, 0.7 V) provides 0.5 V at the operating current to augment the potential for HER and OER on MI and SCII. Because the minimum potential needed to begin the photolysis of water on MI and irradiated SCII is about 0.4 V (the onset po-

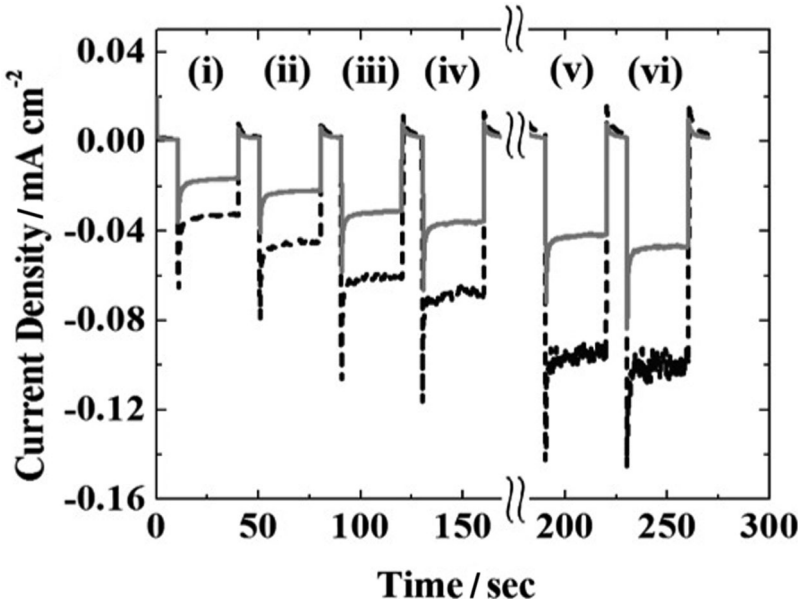

Figure 6. Water-splitting current only using photon energy under different irradiation intensities for i) 120, ii) 180, iii) 270, iv) 310, v) 360, and vi) 410 mW cm^{-2} of UV/Vis (dashed line) and visible (solid line) illumination. Two sets of Pt-W/Mo-$BiVO_4$ and Pt electrodes were used in 0.1 M Na_2SO_4 (pH 7, 0.2 M sodium phosphate buffered) and 25 mM I^-/25 mM IO_3^- solution.

aqueous solution for H_2 and O_2 generation. SCI/MI and SCII/MII were connected by conductive copper tape. For current measurements during the photolysis of water, SCI (or SCII) was used as the working electrode while MI (or MII) was used as the reference and counter electrode for chronoamperometry. The short-circuited condition (zero potential difference between counter/reference lead on MII and working electrode lead on SCII) was employed for the current measurement with no external resistance.

Figure 6 shows the current density for water photolysis resulting from the Z-scheme device using dual Pt-W/Mo-$BiVO_4$ semiconductors. The photocurrent generated from the photon energy is strongly de-

tential of the line i shown in Figure 5) only about 0.1 V from the added 0.5 V is available as electrochemical overpotential ($\eta_{H2/O2}$) to increase the current for the water splitting reaction. For the I^-/IO_3^- redox reactions, about 0.2 V (η_{redox}) is used to drive the current on MII and SCI. Note these overpotentials include a small resistive drop contribution as well.

2.2. Water Photolysis Device

We have shown how two semiconductors of the same material can be combined to fabricate a Z-scheme device for the photolysis of water. Its configuration and electrical contacts between the electrodes are as shown in Figure 3. Photographic images of front–top and side views of the Z-scheme device are shown in the Supporting Information, Figures S2(a) and S2(b). As described above, the device consists of two separate solution reactors: one with NaI/$NaIO_3$ (25 mM/25 mM) redox couple and the other contains a neutral

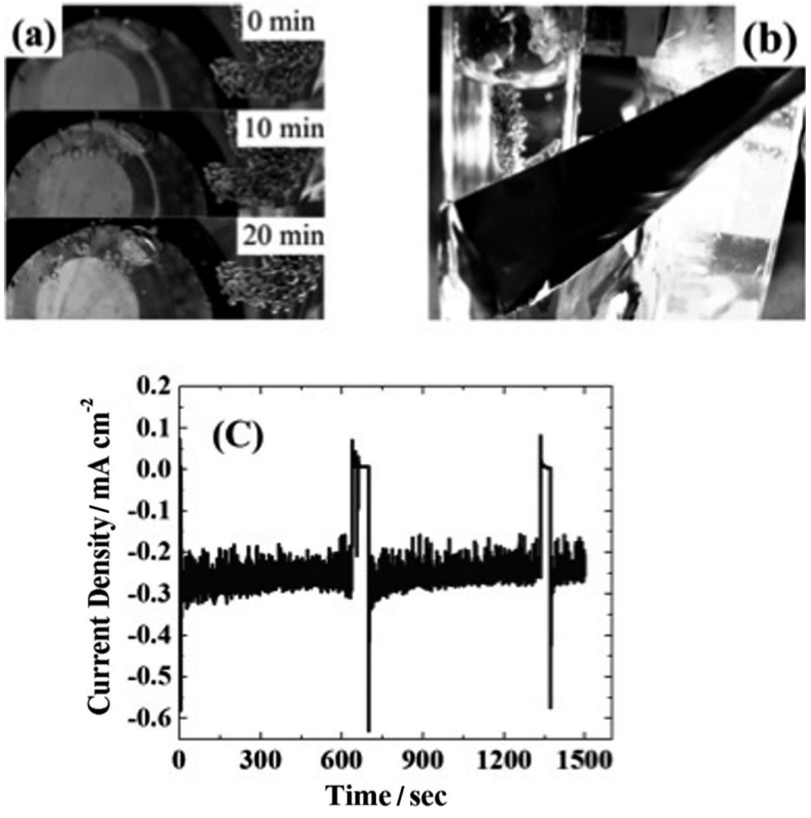

Figure 7. a) Photographic images of bubbles generated on Pt (hydrogen) and Pt-W/Mo-$BiVO_4$ (oxygen) under irradiation and without externally applied potentials. The time shown in the images indicates the duration of irradiation. The large bubbles on the Pt-W/Mo-$BiVO_4$ at 0 min is Ar from the deaeration process before the experiments. b) Side view during the water-splitting experiments. Small bubbles are seen on the Pt electrode in neutral aqueous solution. c) Current density for water splitting under irradiation for 25 min. To take the images shown in (a), irradiation was blocked at about 600 and 1300 s. The UV/Vis illumination intensity was about 400 mW cm^{-2}.

pendent on the illumination intensity and the water-splitting photocurrent increases as the intensity increased. The current density of the water photolysis increases from 0.04 to 0.1 mA cm^{-2} as the intensity of the UV/Vis irradiation increased from 100 mW cm^{-2} to 400 with magnetic stirring of the I^-/IO_3^- redox solution. Also, Figure 6 indicates Pt-W/Mo-$BiVO_4$ utilizes visible irradiation as is expected from the size of the band-gap of Pt-W/Mo-$BiVO_4$, that is, 2.4 eV. The measured current density for water splitting varied from 0.1 to 0.3 mA cm^{-2} (see also Figure 7c) under similar irradiation conditions (intensity of 400 mW cm^{-2}), which is within the scale of estimated current density from the analysis in Figure 5.

In Figure 7, gas bubbles generated on the Pt electrode (H_2) and the Pt-W/Mo-$BiVO_4$ electrode (O_2) were observed and this indicates that the photolysis of water was achieved without externally provided potential. In Figure 7a, development of bubbles on both the Pt-W/Mo-$BiVO_4$ and Pt electrodes are shown as the illumination continued for 20 min. Several small H_2 bubbles produced on the Pt electrode were also clearly observed and released from the electrode into the headspace in Figure 7b. The photocurrent flow was stable for 6 h (inset, Supporting Information Figure S3), which indicates that the material and redox couple (I^-/IO_3^-) are chemically stable for at least this time period.

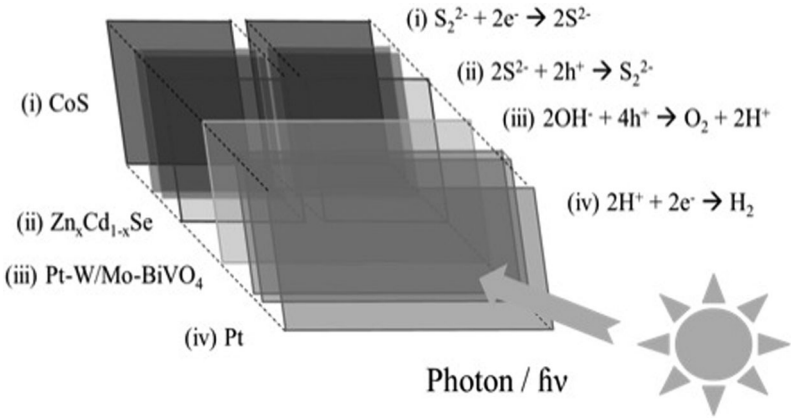

Figure 8. The schematic diagram shows a Z-scheme using $Zn_{0.2}Cd_{0.8}Se$ and Pt-W/Mo-$BiVO_4$ as two absorber materials. The chemical reactions on the electrodes are shown with the corresponding roman numerals for each electrode.

2.3. H_2 Detection

Gas chromatography–mass spectrometry (GC-MS) was used to confirm H_2 generation from the Z-scheme water splitting. The home-built PEC cell for the GC–MS measurements was prepared as shown in the Supporting Information, Figure S1. To prevent O_2 reduction that is generated on Pt-W/Mo-$BiVO_4$ and can impede the proton reduction on Pt, the two electrodes were separated by a glass frit with fine pores in the size range of 10 to 20 μm. However, the glass frit increased the solution resistance to about 600~700 Ω between the two electrodes and induced a potential drop. The potential loss from the solution resistance would be a few tens of mV with the current flow of hundreds of μA. The potential loss is non-negligible considering the overpotential for water splitting of the current device is less than 200 mV. The current flow in the GC-MS cell was thus less than 0.04 mA cm^{-2} because of the high solution resistance (inset, Supporting Information Figure S3) which is about half of that observed in Figure 5. The intensity of the UV-visible irradiation was about 300 mW cm^{-2}. To mitigate the potential drop and still have proper electrode separation, better device engineering is required to reduce the additional potential loss created by the solution resistance and this should be addressed in further studies. However, the current efficiency for H_2 generation from the measured amount of coulombs is about 90% (calculations are shown in Supporting Information Figure S3). The results indicate that most of the photocurrent measured was from the photolysis of water and it is not originating from other reactions such as material decomposition or O_2 reduction reactions.

H_2 generation in the Z-Scheme was also confirmed by the electrochemical detection of hydrogen using a membrane electrode assembly. Membrane electrodes consisting of two Pt/C (40 wt%) electrodes were prepared on a Nafion membrane as described above (Supporting Information, Figure S4a). One side of the membrane electrode faces the headspace of the electrochemical cell where Ar gas (and produced H_2) flows and the other side of the electrode faces air. The two electrodes in this mini-fuel cell were short-circuited and the current was monitored using a potentiostat. The membrane electrode toward the solution was used as the reference and the counter electrode and the electrode facing the air was set as the working electrode. Then, when H_2 bubbles are generated and released from the solution during water photolysis, the H_2 gas reacts on the membrane electrode to generate two protons (H_2 oxidation) on one side of the membrane electrode. As the proton transfers to the other side of the membrane electrode, O_2 reduction occurs to generate water molecules with the transferred protons. Thus, the current flowing through the external circuit demonstrates the generation of H_2 from the water splitting. After about 10 min of irradiation, current was detected on the membrane electrode confirming H_2 generation in the cell (Supporting Information, Figure S4b). The experiment simply simulates the reactions of proton exchange membrane fuel cells and shows the use of converted chemical energy from solar energy. It also confirmed H_2 production from water splitting in the Z-scheme along with the GC–MS measurements.

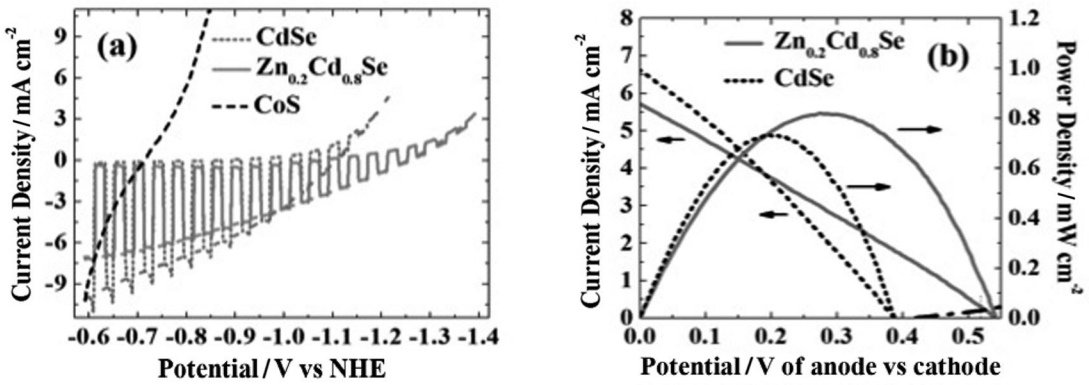

Figure 9. a) LSVs of a CoS electrode for polysulfide reduction and that for sulfide oxidation on $Zn_{0.2}Cd_{0.8}Se$ (solid line) and CdSe (dotted line) under chopped UV/Vis irradiation. The measurements were conducted in 1 M Na_2S, 1 M S, and 1 M KOH aqueous solutions. The light intensity was about 120 mW cm^{-2}. b) Calculated LSVs for the two-electrode configuration, that is, $Zn_{0.2}Cd_{0.8}Se$ (solid line) or CdSe (dotted line) with CoS electrode, from the data shown in (a). The power density of the cell is also calculated from the LSVs. The black dash–dotted line barely seen at the right bottom of (b) shows the current and potential relationship for photolysis of water using Pt-W/Mo-$BiVO_4$ and Pt in a two-electrode configuration.

2.4. $Zn_{0.2}Cd_{0.8}Se$ Photoanode

The Z-scheme device described above using two Pt-W/Mo-$BiVO_4$ electrodes demonstrates the use of two photons with the same semiconductor to boost the potential for water splitting, but it does not utilize the solar radiation with wavelengths longer than 500 nm because of the band gap of W/Mo-$BiVO_4$. $Zn_xCd_{1-x}S_ySe_{1-y}$ is a smaller band gap chalcogenide semiconductors that was investigated by maximizing the photocurrent of Zn–Cd—S–Se compositions by rapid synthesis and screening.[28] To harvest the photon energy with wavelengths longer than 500 nm, $Zn_{0.2}Cd_{0.8}Se$ chalcogenide with a band-gap of about 1.8 eV was prepared as reported previously.[28]

The small-band-gap $Zn_{0.2}Cd_{0.8}Se$ photoanode can be used as described in Figure 8 to absorb that portion of the incident light transmitted through the Pt-W/Mo-$BiVO_4$. Briefly, $Zn_{0.2}Cd_{0.8}Se$ deposited on transparent conductive glass (FTO) oxidizes sulfides and the counter reaction (polysulfide reduction) on a CoS electrocatalyst completes the redox reactions.[42] LSVs of reduction on CoS and oxidation on $Zn_{0.2}Cd_{0.8}Se$ (and for comparison CdSe) are shown in Figure 9a. For the study on the sulfide/polysulfide reaction, a Ag wire was used as a quasi-reference electrode (Ag/Ag_2S) instead of Ag/AgCl because of the instability of porous Vycor glass in a basic solution. However, the potentials reported here are quoted versus the normal hydrogen electrode, Equation (5):

$$Ag_2S + 2e^- \rightarrow 2\ Ag + S^{2-}\ (E^0 = -0.69\ V\ vs.\ NHE) \qquad (5)$$

The reduction and oxidation reactions of polysulfide on CoS are facile enough to obtain a few mA cm^{-2} with only 0.1 V overpotential as shown in Figure 9a(dashed line). $Zn_{0.2}Cd_{0.8}Se$ and CdSe utilize photon energy under irradiation and sulfide oxidation current starts to flow from the potential of −1.1 V for CdSe and from −1.4 V for $Zn_{0.2}Cd_{0.8}Se$. Again, the negative shift of onset potential from −0.7 V (CoS) to −1.1 V (CdSe) shows the utilization of radiation energy by the photoanode. In addition, by adding Zn into CdSe, that is, $Zn_{0.2}Cd_{0.8}Se$, the onset potential of sulfide oxidation shifts to an even more negative value of −1.4 V and the potential shift by Zn doping into CdSe agrees with our previous report on $Zn_xCd_{1-x}S_ySe_{1-y}$.[28] The data presented in Figure 9a are from one of the best performing samples for both CdSe and $Zn_{0.2}Cd_{0.8}Se$ based on the onset potential and the photocurrent at −0.6 V. The current and potential differ somewhat from sample to sample and the film preparation method and the selenization process significantly affects the performance. However, $Zn_{0.2}Cd_{0.8}Se$ usually shows a more negative onset potential and smaller oxidation current than CdSe.

From the LSVs of $Zn_{0.2}Cd_{0.8}Se$ (or CdSe) with CoS, the performance of the PEC galvanic device in a two-electrode configuration and its *I–E* behavior can be drawn as shown in Figure 9b. The open circuit potential, that is, the maximum potential produced from the galvanic device, is the potential difference between the photoanode and the cathode without current flow,

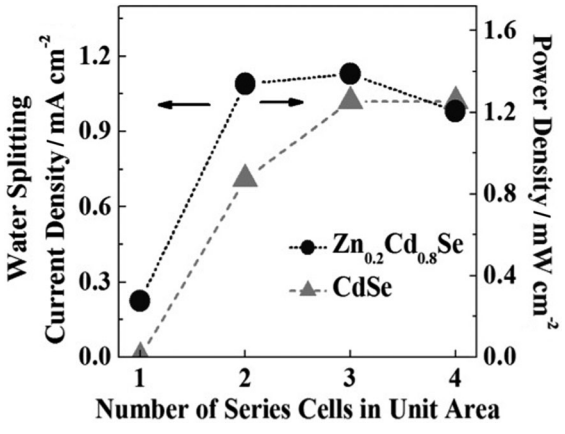

Figure 10. Summary of the analysis discussed in Figure S5 for water splitting using $Zn_{0.2}Cd_{0.8}Se$ (or CdSe) and Pt-W/Mo-$BiVO_4$ photoanodes in a Z-scheme. The calculated current density for the photolysis of water (left axis) and the corresponding power density at operating conditiosn from polysulfide cells (right axis) are shown for different numbers of series-connected $Zn_{0.2}Cd_{0.8}Se$–CoS thin-film electrode cells.

and it is calculated as 0.6 and 0.4 V for $Zn_{0.2}Cd_{0.8}Se$–CoS and CdSe–CoS couples, respectively. The short-circuit current density, that is, the maximum current density that can be obtained from the galvanic cell, is the current density when the $Zn_{0.2}Cd_{0.8}Se$ (or CdSe) has the same electrochemical potential as CoS in Figure 9a. As expected from the LSVs, the $Zn_{0.2}Cd_{0.8}Se$–CoS couple shows higher open circuit potential than the CdSe–CoS couple, and vice versa for the short-circuit current density. Then, from the LSVs calculated in Figure 9b, the current for photolysis of water in the Z-scheme can be estimated as discussed in Figure 5.

The black dotted line in Figure S5b and S5c shows the current and potential relationship for water splitting using Pt-W/Mo-$BiVO_4$ and Pt in a neutral solution. As discussed in Figure 5, the crossing point of the LSVs for the galvanic redox reactions and the water splitting reactions shows the operating current of the Z-scheme device. The water-splitting current is estimated to be as small as 0.1 mA cm^{-2} when a single cell of $Zn_{0.2}Cd_{0.8}Se$–CoS is used and no current flow is estimated when the CdSe–CoS couple is used with the S^{2-}/S_n^{2-} redox reactions (crossing point of gray line and black line in Figures S5b and S5c). Although the maximum power density generated from the S^{2-}/S_n^{2-} redox cell is about 1 mW cm^{-2} with $Zn_{0.2}Cd_{0.8}Se$ and CdSe photoanodes, the power produced by the redox cell cannot be efficiently used for water splitting. This is because the potential produced from the galvanic cell is not large enough for both the H_2 and O_2 evolution; only 0.5 V is produced from the $Zn_{0.2}Cd_{0.8}Se$–CoS couple and 0.4 V from the CdSe–CoS combination.

The available potential from the biasing $Zn_{0.2}Cd_{0.8}Se$–CoS cell can be increased by using several of these. When a single electrode with a constant area is divided into a number of smaller electrodes and they are connected in series as shown in Figure S5a, the potential generated from the series cell can be larger; however, this sacrifices some of the short circuit current density (calculated LSVs as shown Figure S5b and S5c). The maximum power density produced from this series cell at a given light intensity is constant because the total areas of the electrodes are the same. Again, the estimated current density for water photolysis can be obtained from the crossing point of the LSVs for water splitting using Pt-W/Mo-$BiVO_4$ (black line in Figure S5b and S5c) and of S^{2-}/S_n^{2-} redox reactions on $Zn_{0.2}Cd_{0.8}Se$ and CdSe redox cells. The arrows on the right *y* axis in Figure S5b and S5c indicate the power densities at the operating conditions for water splitting with different cell configurations. Figure 10 also summarizes the analysis described above, which shows that two series connections of $Zn_{0.2}Cd_{0.8}Se$ cells can achieve a maximum water splitting photocurrent of about 1 mA cm^{-2} from the system used here.

Based on the analysis discussed in Figures S5 and 10, a PEC device consisting of two pairs of $Zn_{0.2}Cd_{0.8}Se$ photoanodes and a CoS cathode was prepared (Supporting Information, Figure S6). 1 M Na_2S/1 M S in 1 M KOH aqueous solution was used as the redox mediator for the $Zn_{0.2}Cd_{0.8}Se$ and CoS PEC galvanic cells. To minimize both the light absorption by the yellow redox solution and the solution resistance between the two electrodes, the spacing between $Zn_{0.2}Cd_{0.8}Se$ and CoS electrodes was decreased by placing a thin film rubber spacer (Latex, SLR-020-E, Small Parts, Amazon, Seattle, WA) with a thickness of 500 μm between them. After sealing the thin film cell using silicone resin (IS808, GE Silicones, Waterford, NY), the cell was allowed to cure overnight at room temperature. Then, both of the prepared cells were placed behind the Pt-W/Mo-$BiVO_4$ electrode as shown in Supporting Information Figure S6b for chronoamperometry measurements under irradiation.

Chronoamperometry in Figure 11a shows the results of the Z-scheme device utilizing Pt-W/Mo-$BiVO_4$ and the dual split $Zn_{0.2}Cd_{0.8}Se$ photoanode cells. Again, bubble generation of H_2 on Pt and O_2 on Pt-W/Mo-$BiVO_4$ was observed by water splitting (Figure 11b). The photocurrent flowing through the system was about 0.4 mA cm^{-2} under 400 mW cm^{-2} UV/Vis irradiation. However, the power density generated by $Zn_{0.2}Cd_{0.8}Se$ and CoS galvanic cells reported in Figure 9b is only about 1 mW cm^{-2} which limits the maximum conversion efficiency for water splitting to less than 1% with an irradiated photon energy of 120 mW cm^{-2}. The absolute photocurrent or conversion efficiency from photon energy to chemical energy of H_2 evolution is small and far from the best reported efficiencies utilizing buried junction photovoltaic cells (12.4% using *p*-GaAs/p-$GaInP_2$, or 4.7% using triple-junction a-Ge:Si.)[43,44] Moreover, the overpotential of the overall water splitting reaction is still greatly limited by the OER reaction on the Pt-W/Mo-$BiVO_4$ electrode (as shown by the shape of LSVs in Figure 2a and Figure 2b). Therefore, although the enhancement of the photocatalytic activity of the photoanodes has success-

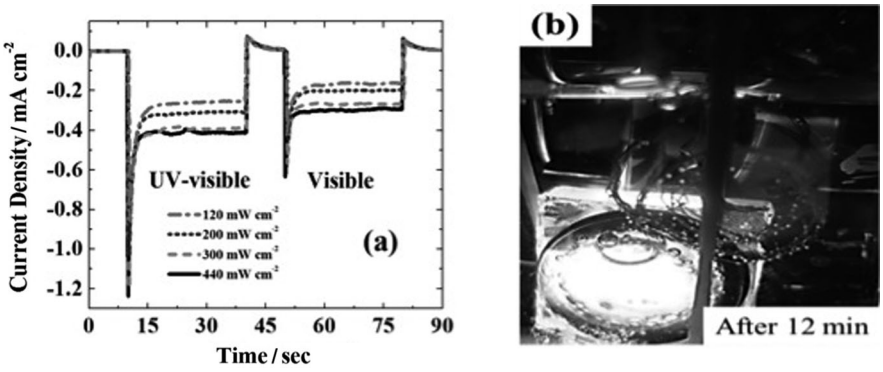

Figure 11. a) Water-photolysis current flow in a Z-scheme using $Zn_{0.2}Cd_{0.8}Se$ and Pt-W/Mo-$BiVO_4$ as two photoanodes under UV/Vis and visible irradiation. Light intensity measurements based on full Xe-lamp outputs of 120 (–•–•), 200 (••••), 300 (----), and 440 mW cm^{-2} (——). A detailed device configuration is shown in the Supporting Information, Figure S6. b) Photographic images taken after 12 min of irradiation (440 mW cm^{-2}, UV/Vis) without any connection to the external equipment. Hydrogen generated on Pt wire and oxygen bubbles on yellow Pt-W/Mo-$BiVO_4$ are observed.

fully been demonstrated for Pt-W/Mo-$BiVO_4$ and $Zn_{0.2}Cd_{0.8}Se$ through the previous studies, the development of highly active photocatalysts is still a limiting factor in practical water photolysis. In addition to material development, engineering the optimization of electrode configurations and cell design is necessary to utilize the converted photon energy efficiently in the device.

Hanna and Nozik considered the performance of pairs of semiconductors in a similar arrangement as described here and proposed that a pair of photoanodes with band gaps of 1.9 and 2.5 eV, could achieve a theoretical solar-to-chemical energy conversion for water splitting of about 10%.[45] In the discussion of Hanna and Nozik, the theoretical conversion efficiency is largely determined by the band-gap size of the photoanodes, the radiant energy obtained from the solar spectrum and electrochemical overpotentials for water splitting. However, both the flat-band position and the size of the band gaps for the photomaterials are important in determining the thermodynamic energy that is obtainable from the radiant energy. As the position of the flat band shifts more positive, the potential gained from the radiation energy at the photoanode decreases. This can result in less favorable conditions for the water splitting. Consequently, one must consider that both the band gap of the semiconductors but also the position of the band edges, the maximum energy from water-splitting products, and the redox couple realize water splitting in a Z-scheme system.

In Figure 12, the position of the band edges of W/Mo-$BiVO_4$ and the redox potentials of the HER and OER are shown. As discussed in connection with Figure 2b, the additional potential that must be applied between the Pt-W/Mo-$BiVO_4$ and the Pt electrodes to initiate water splitting is at least the difference between the conduction-band position of Pt-W/Mo-$BiVO_4$ and the thermodynamic potential of the HER (ΔE_{H2}). Thus, another PEC cell with the redox mediator was used to supply the additional potential in a Z-scheme. The total potential needed in a PEC system is the sum of the thermodynamic energy of water splitting (E_{H2O}) plus an electrochemical driving energy ($\eta_{|H2/O2}$) needed to overcome the activation barrier of H_2 and O_2 generation, and the energy required to drive redox reactions on SCI and MII ($\eta_{|redox}$) at a given current density plus the sum of resistive drops in solution ($\eta_r = iR$), totaling about 2 V.

3. Conclusions

The photocatalytic activity of $BiVO_4$ has been improved by metal doping and surface treatment, for example, W/Mo doping and deposition of the electrocatalyst on the photoanode. The resulting Pt-W/Mo-$BiVO_4$ shows at least a 20-fold improvement in the photoactivity compared to that of untreated $BiVO_4$ for the OER. Using the developed photoanode, preliminary PEC water splitting has been demonstrated without external bias. In the device for the photolysis of water, two n-type semiconductors, namely, Pt-W/Mo-$BiVO_4$ and $Zn_{0.2}Cd_{0.8}Se$, coupled with electrocatalyst electrodes, that is, Pt and CoS, were used to complete the dual n-type-semiconductor (or Z-scheme) water-splitting devices. The Z-scheme configuration consists of two separate electrochemical cells: one with a redox reaction that generates a photopotential and the other for the H_2 and O_2 generation. Two different redox systems were studied. One is the I^-/IO_3^- redox couple for the dual Pt-W/Mo-$BiVO_4$-Pt system, and the other is the S^{2-}/S_n^{2-} redox couple for the $Zn_{0.2}Cd_{0.8}Se$–CoS system. The work herein also exploited the factors that can maximize the utilization of the generated energy from photoanodes for the water splitting. However, less than 1% of irradiated photon energy has been utilized for H_2 generation reactions and the development of more active photoanode material is still a key roadblock to the fabrication of a practical solar-fuel system.

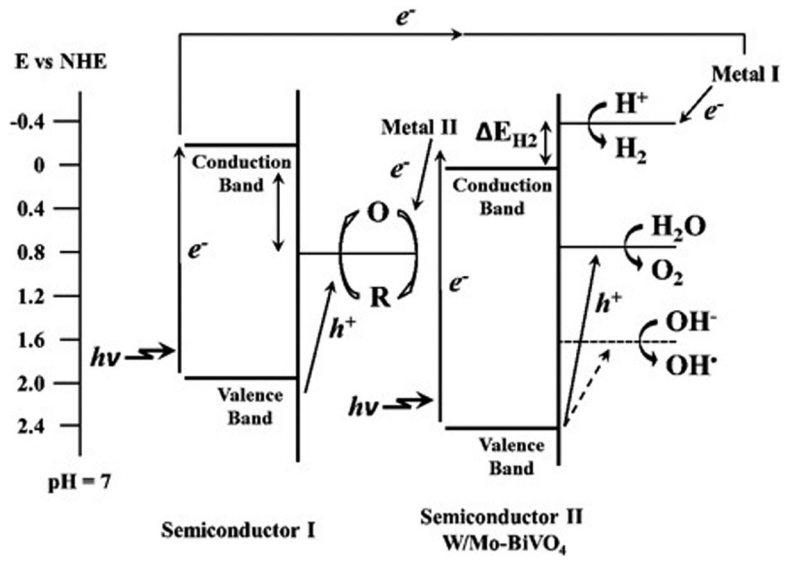

Figure 12. Schematic representations of the electron-transport chain and the redox potentials of the Z-scheme device for the unbiased photolysis of water.

Acknowledgements

This work was funded by the Samsung SAIT GRO Program, the Division of Chemical Sciences, Geosciences, and Biosciences Office of Basic Energy Sciences of the U.S. Department of Energy-SISGR (DE-SC0002219) and the Robert A. Welch Foundation (F-0021).

Keywords: electrochemistry · photoanodes · semiconductors · water splitting · Z-scheme system

[1] A. J. Bard, *Science* **1980**, *207*, 139–144.
[2] A. J. Nozik, *Ann. Rev. Phys. Chem.* **1978**, *29*, 189–222.
[3] A. J. Bard, M. A. Fox, *Acc. Chem. Res.* **1995**, *28*, 141–145.

[4] United States Department of Energy, *a National Vision of America's Transition to a Hydrogen Economy To 2030 and Beyond*, February, **2002**.
[5] A. Fujishima, K. Honda, *Nature* **1972**, *238*, 37 – 38.
[6] W. J. Youngblood, S.-H. A. Lee, K. Maeda, T. E. Mallouk, *Acc. Chem. Res.* **2009**, *42*, 1966 – 1973.
[7] L. Li, L. Duan, Y. Xu, M. Gorlov, A. Hagfeldt, L. Sun, *Chem. Commun.* **2010**, *46*, 7307 – 7309.
[8] R. Brimblecombe, A. Koo, G. C. Dismukes, G. F. Swiegers, L. Spiccia, *J. Am. Chem. Soc.* **2010**, *132*, 2892 – 2894.
[9] W. Y. Teoh, J. A. Scott, R. Amal, *J. Phys. Chem. Lett.* **2012**, *3*, 629 – 639.
[10] C. Ng, A. Iwase, Y. H. Ng, R. Amal, *J. Phys. Chem. Lett.* **2012**, *3*, 913 – 918.
[11] T. Nann, S. K. Ibrahim, P.-M. Woi, S. Xu, J. Ziegler, C. J. Pickett, *Angew. Chem.* **2010**, *122*, 1618 – 1622; *Angew. Chem. Int. Ed.* **2010**, *49*, 1574 – 1577.
[12] M. G. Walter, E. L. Warren, J. R. McKone, S. W. Boettcher, Q. Mi, E. A. Santori, N. S. Lewis, *Chem. Rev.* **2010**, *110*, 6446 – 6473.
[13] S. W. Boettcher, E. L. Warren, M. C. Putnam, E. A. Santori, D. Turner-Evans, M. D. Kelzenberg, M. G. Walter, J. R. McKone, B. S. Brunschwig, H. A. Atwater, N. S. Lewis, *J. Am. Chem. Soc.* **2011**, *133*, 1216 – 1219.
[14] R. E. Rocheleau, E. L. Miller, A. Misra, *Energy Fuels* **1998**, *12*, 3 – 10.
[15] K. Sivula, F. Le Formal, M. Gratzel, *ChemSusChem* **2011**, *4*, 432 – 449.
[16] S. Cervera-March, E. S. Smotkin, A. J. Bard, A. Campion, M. A. Fox, T. Mallouk, S. E. Webber, J. M. White, *J. Electrochem. Soc.* **1988**, *135*, 567 – 573.
[17] E. Smotkin, A. J. Bard, A. Campion, M. A. Fox, T. Mallouk, S. E. Webber, J. M. White, *J. Phys. Chem.* **1986**, *90*, 4604 – 4607.
[18] E. S. Smotkin, S. Cervera-March, A. J. Bard, A. Campion, M. A. Fox, T. Mallouk, S. E. Webber, J. M. White, *J. Phys. Chem.* **1987**, *91*, 6 – 8.
[19] A. J. Bard, *J. Photochem.* **1979**, *10*, 59 – 75.
[20] K. Maeda, M. Higashi, D. Lu, R. Abe, K. Domen, *J. Am. Chem. Soc.* **2010**, *132*, 5858 – 5868.
[21] J. E. Katz, T. R. Gingrich, E. A. Santori, N. S. Lewis, *Energy Environ. Sci.* **2009**, *2*, 103 – 112.
[22] M. Woodhouse, G. S. Herman, B. A. Parkinson, *Chem. Mater.* **2005**, *17*, 4318 – 4324.
[23] J. S. Jang, J. Lee, H. Ye, F.-R. F. Fan, A. J. Bard, *J. Phys. Chem. C* **2009**, *113*, 6719 – 6724.
[24] J. He, B. A. Parkinson, *ACS Comb. Sci.* **2011**, *13*, 399 – 404.
[25] S. Jang, K. Y. Yoon, X. Xiao, F.-R. F. Fan, A. J. Bard, *Chem. Mater.* **2009**, *21*, 4803 – 4810.
[26] S. H. Baeck, T. F. Jaramillo, C. Brandli, E. W. McFarland, *J. Comb. Chem.* **2002**, *4*, 563 – 568.
[27] W. Liu, H. Ye, A. J. Bard, *J. Phys. Chem. C* **2010**, *114*, 1201 – 1207.
[28] H. Ye, J. Lee, J. S. Jang, A. J. Bard, *J. Phys. Chem. C* **2010**, *114*, 13322 – 13328.
[29] H. S. Park, K. E. Kweon, H. Ye, E. Paek, G. S. Hwang, A. J. Bard, *J. Phys. Chem. C* **2011**, *115*, 17870 – 17879.
[30] G. Liu, C. Liu, A. J. Bard, *J. Phys. Chem. C* **2010**, *114*, 20997 – 21002.
[31] G. Liu, A. J. Bard, *J. Phys. Chem. C* **2010**, *114*, 17509 – 17513.
[32] S. C. Riha, B. A. Parkinson, A. L. Prieto, *J. Am. Chem. Soc.* **2011**, *133*, 15272 – 15275.
[33] A. Kudo, K. Omori, H. Kato, *J. Am. Chem. Soc.* **1999**, *121*, 11459 – 11467.
[34] J. A. Seabold, K.-S. Choi, *J. Am. Chem. Soc.* **2012**, *134*, 2186 – 2192.
[35] D. K. Zhong, S. Choi, D. R. Gamelin, *J. Am. Chem. Soc.* **2011**, *133*, 18370 – 18377.
[36] P. J. Bridge, M. W. Pryce, *Mineral. Mag.* **1974**, *39*, 847 – 849.
[37] K. Sayama, A. Nomura, T. Arai, T. Sugita, R. Abe, M. Yanagida, T. Oi, Y. Iwasaki, Y. Abe, H. Sugihara, *J. Phys. Chem. B* **2006**, *110*, 11352 – 11360.
[38] H. Ye, H. S. Park, A. J. Bard, *J. Phys. Chem. C* **2011**, *115*, 12464 – 12470.
[39] M.-G. Kim, M. G. Kanatzidis, A. Facchetti, T. J. Marks, *Nat. Mater.* **2011**, *10*, 382 – 388.
[40] R. Abe, K. Sayama, H. Sugihara, *J. Phys. Chem. B* **2005**, *109*, 16052 – 16061.
[41] A. J. Bard, L. R. Faulkner, *Electrochemical Methods Fundamentals and Application, 2nd ed.;* John Wiley & Sons, New York, **2001**.
[42] P. M. Lessner, F. R. McLarnon, J. Winnick, E. J. Cairns, *J. Electrochem. Soc.* **1993**, *140*, 1847 – 1849.
[43] O. Khaselev, J. A. Turner, *Science* **1998**, *280*, 425 – 427.
[44] S. Y. Reece, J. A. Hamel, K. Sung, T. D. Jarvi, A. J. Esswein, J. J. Pijpers, D. G. Nocera, *Science* **2011**, *334*, 645 – 648.
[45] M. C. Hanna, A. J. Nozik, *J. Appl. Phys.* **2006**, *100*, 074510.

Received: December 13, 2012
Published online on March 12, 2013